NeuroImage 113 (2015) 37–43

Contents lists available at ScienceDirect

NeuroImage

journal homepage: www.elsevier.com/locate/ynimg

fMRI contrast at high and ultrahigh magnetic fields: Insight from complementary methods

Luisa Ciobanu [a,1], Eddy Solomon [b,1], Nadya Pyatigorskaya [a], Tangi Roussel [b], Denis Le Bihan [a], Lucio Frydman [b,*]

[a] NeuroSpin, Commissariat à l'Energie Atomique et aux Energies Alternatives, Gif-sur-Yvette, France
[b] Weizmann Institute of Science, Rehovot, Israel

ARTICLE INFO

Article history:
Received 12 December 2014
Accepted 9 March 2015
Available online 18 March 2015

Keywords:
Ultrahigh fields
Functional MRI
Spatiotemporal encoding
BOLD activation
T1 contrast
Forepaw stimulation

ABSTRACT

This manuscript examines the origins and nature of the function-derived activation detected by magnetic resonance imaging at ultrahigh fields using different encoding methods. A series of preclinical high field (7 T) and ultra-high field (17.2 T) fMRI experiments were performed using gradient echo EPI, spin echo EPI and spatio-temporally encoded (SPEN) strategies. The dependencies of the fMRI signal change on the strength of the magnetic field and on different acquisition and sequence parameters were investigated. Artifact-free rat brain images with good resolution in all areas, as well as significant localized activation maps upon forepaw stimulation, were obtained in a single scan using fully refocused SPEN sequences devoid of T2* effects. Our results showed that, besides the normal T2-weighted BOLD contribution that arises in spin-echo sequences, fMRI SPEN signals contain a strong component caused by apparent T1-related effects, demonstrating the potential of such technique for exploring functional activation in rodents and on humans at ultrahigh fields.

Introduction

Nuclear magnetic resonance (NMR) in general, and NMR imaging (MRI) in particular, have steadily benefited from continuous increases in the static magnetic field B_0 at which these experiments are performed. These increases provide higher resolution and better sensitivity, both in spectral characterization and in spatial imaging. Counted among the latter's main areas of application are functional (fMRI) studies, one of the basic keystones of modern neuroimaging. fMRI techniques are generally used to record neuronal activities in different regions, when brains or other targeted organs are subjected to different paradigmatic stimuli (Heeger and Ress, 2002; Norris, 2006). In terms of mapping the origins of these functional stimuli, the most commonly employed fMRI acquisition strategy is single-shot gradient-echo echo-planar-imaging (GE-EPI). This sequence highlights alterations in neuronal activity based on hemodynamic changes affecting the relaxation parameter T2* (Chavhan et al., 2009; Logothetis and Wandell, 2004), via a mechanism known as the blood oxygen level dependent (BOLD) effect. Although providing the strongest observables in fMRI activation experiments, T2*-based methods can exhibit a number of drawbacks. One of these relates to the relatively low resolution activation maps that these methods usually generate, reflecting static long-range dephasing effects deriving from major vein systems (Ogawa and Lee, 1990; Ogawa et al., 1993). Additionally, more serious limitations arise as magnetic fields are increased—particularly when investigating brain areas located near air–tissue interfaces, such as the orbitofrontal and the inferior temporal lobes. In such cases, the same T2* mechanism lying at the basis of the functional characterization can lead to a rapid signal dephasing and to potentially important image distortions and sensitivity losses, driven by local magnetic susceptibility changes. One possible way to alleviate these constraints is by resorting to further optimizations of the GE-EPI experiment, involving for instance tilted-slices acquisition, parallel acquisition strategies and restricted field of views (Deichmann et al., 2003; Heidemann et al., 2012). Yet another option relies on using spin echo (SE) imaging techniques, which remove both of these static, T2*-like effects (Ugurbil et al., 1999). The SE improvement in the spatial definition and its restoration of signal losses in the MR images (Norris et al., 2002; Schwarzbauer et al., 2010; Weiskopf et al., 2006), however, will usually be achieved at the expense of a partial loss and/or change in the functional contrast. Recently, another option was assessed in the acquisition of fMRI data, based on the *spa*tiotemporal *en*coding (SPEN) of the imaging data (Airaksinen et al., 2010; Ben-Eliezer et al., 2012; Goerke et al., 2011). SPEN is a novel spin manipulation technique capable of delivering arbitrary multidimensional NMR spectra or MRI images in a single scan (Tal and Frydman, 2010). At the core of SPEN lies replacing the conventional time- or phase-

Abbreviations: BOLD, blood-oxygen-level dependent; EPI, echo planar imaging; fMRI, functional MRI; FOV, field of view; GE, gradient echo; MRI, magnetic resonance imaging; NMR, nuclear magnetic resonance; SAR, specific absorption rate; SE, spin echo; SPEN, spatio-temporal encoding; SR, super-resolution.

* Corresponding author at: Chemical Physics Department, Weizmann Institute, 76100 Rehovot, Israel.
E-mail address: lucio.frydman@weizmann.ac.il (L. Frydman).

[1] These authors contributed equally to this work.

http://dx.doi.org/10.1016/j.neuroimage.2015.03.018
1053-8119/

encoding increments used in nD NMR/MRI, by an encoding implemented using frequency-swept (chirped) pulses executed under the action of field gradients (Kunz, 1986; Pipe, 1995). When considered in a real-time, single-shot MRI setting, SPEN involves replacing the EPI excitation by a linear frequency chirped excitation (or refocusing) pulse, applied in the presence of an encoding gradient G_{exc}. Performing this along the low-bandwidth axis and sampling the orthogonal dimension using a conventional read-out gradient, result in a "hybrid" approach with a number of interesting, advantageous features. Being free from traditional Nyquist considerations, hybrid-SPEN can provide significantly higher immunity to B_0-inhomogeneities and chemical-shift offsets than EPI counterparts: it enables working with stronger encoding gradients, as well as zooming in particular regions of interest. Another feature of SPEN relates to the fact that it can deliver images that are "fully refocused" vis-à-vis T2* effects, throughout the entire course of the data acquisition (Ben-Eliezer et al., 2010; Chamberlain et al., 2007). This is in contrast with SE-EPI acquisitions, where static inhomogeneities only cancel at an instant corresponding to the chosen echo time TE. Fully-refocused SPEN is achievable by an appropriate timing of the encoding and acquisition segments, requiring these times to be of equal duration if the encoding is executed using a 90° chirp pulse, and to differ by a factor of 2 if the encoding was implemented by an inversion swept pulse. By freeing its images of T2*-like effects, this acquisition mode can render SPEN even more insensitive to static field distortions, making it particularly promising for accessing challenging organs or tissue areas in ultrahigh field studies.

An interesting aspect concerning these various single-shot acquisition approaches lies in their potential performance as fMRI probes in high magnetic field investigations. Increases in magnetic fields have given unambiguous improvements in certain spectroscopic and imaging experiments, but their payoff in fMRI studies remains to be fully assessed. Certain factors such as the shortening in T2 and the increase in T1 that water protons usually undergo with magnetic field (Bandettini et al., 2012; de Graaf et al., 2006), might conspire against conventional sensitivity expectations. On the other hand, new contrasts may arise that compensate for these compromises. Driven by this promise, fMRI's signal-to-noise and contrast-to-noise considerations at ultrahigh fields have been the focus of attention in both animal and humans studies (Logothetis, 2008; Norris, 2006, 2012; Ugurbil, 2012; Ugurbil et al., 1999). These works have generally shown that given the increased distortions arising at higher magnetic fields, SE or combinations of GE and SE scans are the preferred options from the standpoint of image quality. Under these conditions static T2*-based effects cease dominating the functional contrast, and begin competing with T2-like dephasings arising from changes in the natural relaxation times and from dynamic effects within the arterial and venous vasculatures. These results imply that ultrahigh field fMRI can be a very promising option, even if an exact interpretation of such data remains to be elucidated as the fMRI contrast appears to depend on the acquisition method and paradigms used (Frahm et al., 1994; Kim et al., 1994).

The goal of this work is to further examine the nature of the function-derived activation observed at high (7 T) and ultra-high (17.2 T) magnetic fields, when relying on methods that are based mostly on T2* (GE), on a mixture of T2 and T2* (SE), and fully-freed from T2* effects (fully refocused SPEN). Towards this end a variety of fMRI studies were performed on rodents, focusing on brain hyperoxia and on pinpointing areas of localized activation upon subjecting the animals to forepaw stimulation. Our data show that, besides the expected image quality improvement delivered by T2*-free SPEN scans over EPI counterparts, these scans are indeed free from the T2*-weighted BOLD contributions which dominate GE (and to some extent SE) sequences. In addition, fMRI SPEN results suggest that an additional contribution arises at ultrahigh fields, which adds to the retrieval of very clear functional maps observed even under full refocusing conditions. This contribution could be traced to apparent T1-related effects, as fMRI responses could be modulated by varying the scanning repetition rate, and/or changing the T1 relaxation time by repeating measurements at 7 T and 17.2 T. Potential explanations and consequences for these findings in MRI-based functional neuroimaging are briefly discussed.

Methods

Animal preparation

Hyperoxia and fMRI experiments were performed on 21 male Sprague–Dawley rats (200–250 g, Janvier Labs, Saint Berthevin, France). The rats were housed two per cage under controlled light conditions (7:00–19:00), and were given free access to water and food. All animal procedures used in the present study were approved by the Comité d'Ethique en Expérimentation Animale, Commissariat à l'Energie Atomique et aux Énergies Alternatives, Direction des Sciences du Vivant (Fontenay-aux-Roses, France). Out of the 21 animals, 5 were used for hyperoxia experiments and 16 for fMRI. During all MRI exams the respiration rate and body temperature were monitored. The body temperature was maintained between 36.5 and 37 °C using heated water (Grant TC120, WPI, Hitchin, UK) or air (model 1025; SA Instruments, Stony Brook, NY) circuit devices. To avoid motion-related artifacts the head was immobilized using a bite bar and ear pins.

Hyperoxia

For all hyperoxia experiments the animals were intubated and mechanically ventilated (MRI ventilator, Bioseb, Vitrolles Cedex, France) while anesthetized with 2% isoflurane. The expired CO_2 was monitored using a MicroCapStar CO_2 monitor (Bioseb, Vitrolles Cedex, France). 5 min after the beginning of the acquisition, medical air was replaced by 100% oxygen for 5 min, before switching again to air for another 5 min, accounting for a total acquisition time of 15 min.

Functional imaging

During the fMRI experiments an air–oxygen gas mixture (20% oxygen in medical air) was delivered to a nose-cone mask for spontaneous respiration. The animals were anesthetized initially with 5% isoflurane, which was reduced to 2% for maintenance. After insertion of the needle electrodes used in electrical forepaw stimulation experiments, a bolus of 0.05 mg/kg medetomidine (Domitor, Pfizer, Karlsruhe, Germany) was injected subcutaneously, and isoflurane was disconnected 10 min later. A continuous subcutaneous infusion of medetomidine (0.1 mg/kg/h) was started 15 min after the bolus injection. To perform the electrical forepaw stimulation, two pairs of needle electrodes (26 gauge) were inserted under the skin of the right and left forepaws (between digits 2 and 3 and digits 4 and 5). Either the right or the left paw was used for each fMRI acquisition. Electrical pulse stimulation was given with a constant current bipolar isolated pulse stimulator (model 2100; A-M Systems, Sequim, WA), triggered by a transistor–transistor logic pulse from the Bruker imaging system. Rectangular pulses with 3-ms duration, 2-mA current and 10 Hz frequency (100-ms interval) were applied five times for 30 s, separated by a 30-s rest interval. A 10 minute delay was maintained between consecutive fMRI runs.

MRI procedures

MRI experiments were performed at magnetic field strengths of 7 T and 17.2 T, on horizontal scanners (Bruker BioSpin, Ettlingen, Germany) equipped with gradient systems allowing maximum gradient strengths of 760 and 1000 mT/m, respectively. Surface coils (30 mm diameter loops) were used for transmission and reception. For positioning the targeted field-of-view (FOV), multislice fast low angle shot (FLASH) images were acquired. Good B_0 homogeneity was ensured through automatic iterative FASTMAP methods (ParaVision 5.1), followed by a MAPSHIM correction (Gruetter, 1993; Kanayama et al., 1996) in the region of interest. Hyperoxia experiments were performed using spin-echo single shot echo-planar imaging (SE-EPI, Fig. 1a) and two hybrid

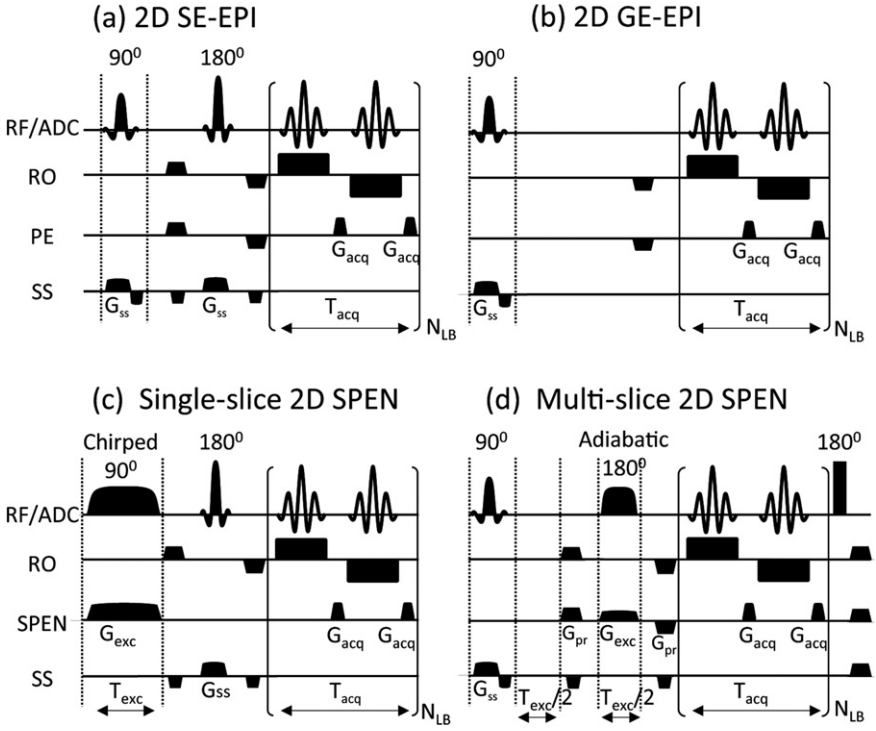

Fig. 1. Diagrams of the single-shot pulse sequences used: (a) 2D SE-EPI, (b) 2D GE-EPI, (c) single-slice 2D 90°-based hybrid SPEN and (d) multi-slice 2D 180°-based hybrid SPEN. Abbreviations denote the following: G_{exc}: excitation gradient, G_{acq}: acquisition gradient, G_{ss}: slice-selection gradient, T_{exc}: excitation time, T_{acq}: acquisition time, RF/ADC: irradiation and acquisition channel, RO: readout axis, PE: phase-encoding axis, SPEN: SPatiotemporal ENcoding axis, SS: slice-selection axis, and N_{LB}: number of loops of phase/spatiotemporally-encoded lines executed along these low-bandwidth dimensions. Both SPEN sequences were implemented in the fully refocused mode ($T_{exc} = T_{acq}$).

SPEN acquisition schemes based on 90°- and 180° frequency-swept encoding pulses ($SPEN_{90}$ and $SPEN_{180}$; Figs. 1c and d, respectively) (Ben-Eliezer and Frydman, 2011; Schmidt and Frydman, 2014). fMRI data were acquired using gradient echo echo-planar imaging (GE-EPI, Fig. 1b) and 90°-based $SPEN_{90}$ techniques. The hybrid SPEN sequences used were custom written and can be freely downloaded from ftp://ftp.weizmann.ac.il/incoming/spen.install.package.tar.gz. Typical acquisition parameters were as follows: data matrix size: 100 × 100 pixels, FOV: 2 cm × 2 cm; slice thickness: 1.2 mm; bandwidth (BW): 400 and 357 kHz at 17.2 T and 7 T, respectively; and repetition time (TR): 10 s (hyperoxia), 1.5 s and 3 s (fMRI). SPEN parameters: To achieve the fully refocused conditions the excitation pulse and acquisition duration for the $SPEN_{90}$ experiment were set equal; i.e., T_{acq}: 25 ms; $T_{exc,90°\text{-}chirp}$: 25 ms, and BW: 5 kHz. Achieving similar conditions in the $SPEN_{180}$ experiment required setting the refocusing pulse to half the acquisition duration; i.e., T_{acq}: 20 ms; $T_{180°\text{-}chirp}$: 10 ms, and BW: 10 kHz. As a result of these choices the echo times were nearly identical (TE: 30–32 ms) for all three methods in the hyperoxia experiments. Echo times for other experiments were 11 ms (GE-EPI, 7 T) and 10 ms (GE-EPI, 17.2 T). For fMRI GE-EPI three coronal slices were acquired, which included the primary and secondary somatosensory cortex. One of the activated slices was chosen for the 2D SPEN acquisitions.

Data processing and analysis

SPEN data was reconstructed using in-house Matlab (Matworks, Natick, MA) image-reconstruction algorithms based on super-resolution (SR) principles (Chen et al., 2013; Jing Li et al., 2014). It has been shown that this enables to recoup the sensitivity and spatial resolution losses, that for similar acquisition gradient strengths and acquisition times SPEN will otherwise evidence vis-à-vis EPI (Ben-Eliezer et al., 2014). These processing algorithms are also incorporated in the Paravision method, and are downloadable from ftp://ftp.weizmann.ac.il/incoming/spen.install.package.tar.gz.

Functional imaging analysis

SPM8 software (Wellcome Trust Centre for Neuroimaging, London, UK) was used for fMRI data processing, including slice realignment. Image sets containing clear motion artifacts or head movement were discarded. Activation maps were calculated using SPM8 and plotted at a threshold of $p < 0.05$. Average percent fMRI signal changes were calculated from 9 pixels chosen in the center of the active area. The statistical comparison between the number of active voxels and the fMRI signal change for different experimental conditions (strength of magnetic field and repetition time) was performed using bilateral paired Student *t*-tests.

Hyperoxia data analysis

Three pulse sequences were used in the hyperoxia studies: SE-EPI, $SPEN_{90}$ hybrid sequences based on 90° chirped excitations, and $SPEN_{180}$ hybrid sequences based on 180° swept inversions. The expected signal intensity changes induced by hyperoxia on each of these sequences were calculated, in order to validate the correctness of our fMRI analysis assumption. For SE-EPI the time domain signal is mainly dictated by T2 and T2* relaxation, and can be expressed as:

$$S(t)\approx\begin{cases} e^{-R_2\cdot t}\cdot e^{-R_2^*\cdot(\mathrm{TE}-\mathrm{t})}, & 0\le \mathrm{t}\le \mathrm{TE} \\ e^{-R_2\cdot \mathrm{t}}\cdot e^{-R_2^*(\mathrm{t}-\mathrm{TE})}, & \mathrm{TE}\le \mathrm{t}\le \frac{3}{2}\cdot \mathrm{TE} \end{cases} \quad (1)$$

with $R_2 = \frac{1}{T_2}$ and $R_2^* = \frac{1}{T_2^*}$. In the case of the fully refocused SPEN experiments we assumed that the images were essentially free from T2* effects. Signal intensities are thus solely T2 dependent and their dependence along the low-bandwidth dimension can be written as: $S_{SPEN_{180}}(t)\approx e^{-R_2 t}$, $T_{acq}\le t\le 2T_{acq}$ and $S_{SPEN_{90}}(t)\approx e^{-R_2 t}$, $0\le t\le 2T_{acq}$; for the 180°- and 90°-based SPEN, respectively (here T_{acq} represents the acquisition time, which is equal to the duration of the 90° pulse and twice the duration of the 180° for fully refocused sequences). The hyperoxia signal change, regardless of the sequence used, was

calculated as $\Delta I_{calc} = \frac{I_{o_2} - I_{air}}{I_{air}}$, where I denotes a given pixel image intensity and the subindices denote air and 100% O_2 replacement periods. Here a distinction needs to be introduced between EPI that carries out the image acquisition in the k-domain, and SPEN which does so in direct physical space: $I = FT[S(t)]$ for SE-EPI and $I \propto Abs[S(t)]$ for SPEN (with the exact proportionality details depending on the super-resolution algorithm employed for the image reconstruction). Experimentally, we calculated the average signal change in a similar fashion: $\Delta I_{\exp} = \frac{\bar{I}_{o_2} - \bar{I}_{air}}{\bar{I}_{air}}$, where $\bar{I}_{air}$ and $\bar{I}_{o_2}$ are the average signal intensities from repeated experiments.

Results

Image quality

Fig. 2 compares representative SE-EPI and SPEN images, acquired on the same animal at 17.2 T. Due to magnetic susceptibility mismatches the SE-EPI image exhibits image artifacts in the close vicinity of the primary motor cortex (yellow arrows, Fig. 2a) and signal losses in the lower part of the brain (red arrows, Fig. 2a). The SPEN acquisition substantially improves the quality of these images (Fig. 2b), recovering most of the signal loss and eliminating the distortions. In addition, signal intensities are generally larger in the latter experiments, thanks for the T2* refocusing provided by the full refocusing conditions. Similar qualities could be retrieved with suitably timed single-scan SPEN sequences based on 180° swept pulses.

Hyperoxia

As mentioned, the neuronal activation features detected in fMRI are usually affected by the type of imaging sequence used. fMRI signals acquired using GE-EPI and SE-EPI are typically influenced by stronger and weaker T2* effects, respectively. Probing fMRI using fully-refocused SPEN raises questions as to the origin of the functional signal that will emerge in this approach, which in principle refocuses all T2* relaxation effects that lie at the basis of BOLD. Although similar considerations were raised in experiments carried out using RASER (Ben-Eliezer et al., 2012; Goerke et al., 2011), we decided to further clarify this by investigating the fMRI responses observed for SE-EPI and for SPEN-based methodologies, on animals submitted to hyperoxia. This is a well-known paradigm that mimics the BOLD response in the absence of neuronal activation, by virtue of the diamagnetic character gained by hemoglobin upon oxygenation. The results of these comparisons are summarized in Fig. 3, which shows representative signal change maps measured using different pulse sequences. As expected, all experiments reveal an increase in signal intensity in all brain areas affected by the hyperoxia challenge. Also as expected, the SE-EPI sequence yielded – within the bounds of the MR coil's non-uniform detection and of heterogeneities in the anatomical features – hyperoxia signal changes that varied the least across the brain (Fig. 3a). SPEN imaging approaches, by contrast, yielded changes in signal intensities exhibiting a stronger dependence on the voxels' position along the SPEN-encoded axis (Figs. 3b, c). Quantitative analyses of these changes (Figs. 3e, f, g) indicate that the hyperoxia-derived signal intensity changes are both strongest and most spatially dependent in the case of $SPEN_{90}$ experiments. These plots also confirm that the simple models introduced in the Methods section can account for these functional behaviors, including for the spatial dependence of the SPEN signal along the low-bandwidth direction, and for the stronger spatial dependence and inhomogeneity exhibited by the $SPEN_{90}$ experiments. Discrepancies are still clear between the experiments and the simple model in Eq. (1), but these are mainly due to signal intensity variations caused by field inhomogeneities and anatomical features. For the $SPEN_{90}$ based sequences the functional variation of the signal can thus be traced solely to T2 changes, coupled to the time differences each isochromat experiences between its instant of excitation/refocusing until the time it delivers its echo: spins that are excited first are detected last (or vice versa), and hence are subject to the biggest (smallest) decay changes. (Notice that this is at variance with other SPEN strategies such as RASER (Chamberlain et al., 2007) where all spin packets experience the same TE). These features are further stressed in Figs. 3d and h, which show how the heterogeneities of $SPEN_{90}$'s hyperoxia signal maps reverse when the sweep direction of the chirp pulse executing the encoding is reversed. Interestingly, these results also evidence that at these high fields, the changes in T2 induced by the blood oxygenation, give sufficient contrast to compete successfully against sequences that like SE-EPI, are more heavily biased by T2* effects. This is probably a reflection of the T2 shortening that occurs as magnetic fields are increased, and which eventually may mask the contributions of T2* changes (de Graaf et al., 2006). Thus, even though fully refocused and thus largely free from T2* effects, SPEN sequences appear at these high fields as potential routes worth exploring in fMRI.

Functional MRI

Fig. 4 displays typical GE-EPI and SPEN activation maps obtained from a forepaw stimulation paradigm, overlaid on the average single-scan images acquired at 17.2 T and 7 T during the course of these functional tasks. Even though devoid of T2* contributions, the fully refocused SPEN image observed for TR = 1.5 s yields strong, localized activation maps with good t-score levels (Figs. 4b and e). The magnitude

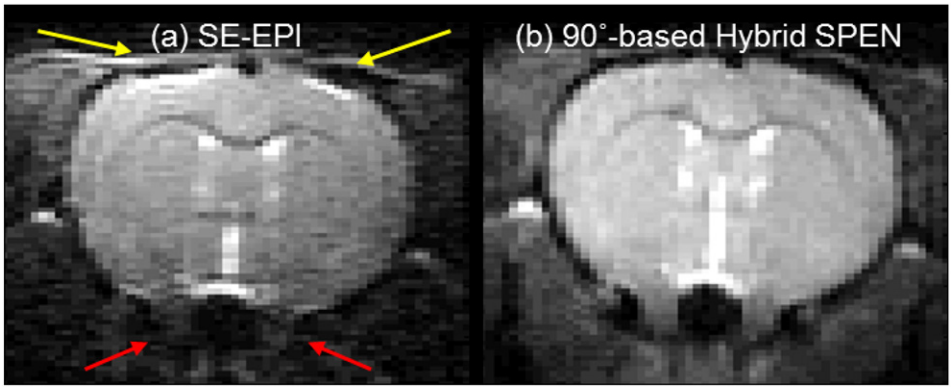

Fig. 2. Comparison between rat brain images (coronal view) acquired at 17.2 T using SE-EPI (a) and fully-refocused 90°-based hybrid SPEN (b) acquisition schemes. The geometric distortions in the cortex region (yellow arrows) and signal loss in the lower part of the brain (red arrows) generated by the EPI are eliminated when using SPEN. In plane image resolution: 200 × 200 μm. Slice thickness: 1.2 mm. See Methods for further details.

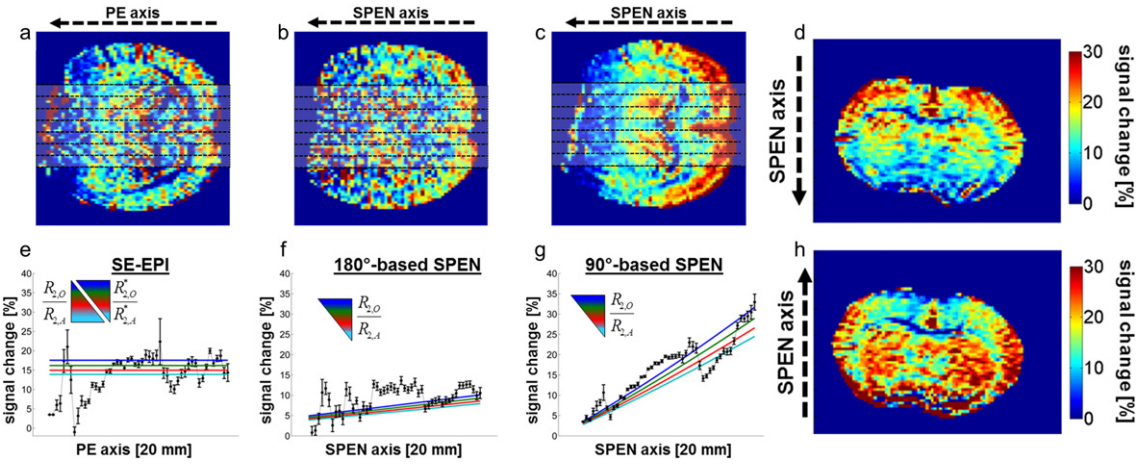

Fig. 3. Hyperoxia-induced signal intensity change maps for: SE-EPI (a), 180°-based SPEN (b) and 90°-based hybrid SPEN (c). Experimental data projected in the low-bandwidth dimension (symbols), compared against expected signal (solid colored lines) for: SE-EPI (e), 180°-based hybrid SPEN (f) and 90°-based hybrid SPEN (g). The calculations were performed as described in Methods for four different $R_{2,oxygen}/R_{2,air}$ and $R_{2*,oxygen}/R_{2*,air}$ ratios colored blue, green, red and magenta respectively: 0.887/0.891, 0.891/0.895, 0.895/0.899, and 0.898/0.902 (all values in Hz). Error bars represent standard deviations. Panels (d) and (h) show how the hyperoxia signal intensity maps change upon reversing the sense of sweep for $SPEN_{90}$'s initial 90° encoding pulse, as indicated by the arrows. In plane image resolution: 200 × 200 μm. Slice thickness: 1.2 mm.

of the 17.2 T activation changes possess, on average, ca. 50% the intensity of the one originated by the BOLD-based GE-EPI sequence; while at 7 T the levels of activation are comparable. Increasing SPEN's TR from 1.5 s to 3 s substantially reduces the number of active pixels at both magnetic field strengths (see Figs. 4c, f and Tables 1, 2 in the Supplementary Material for a description of the fMRI signal intensity changes and changes in size of active areas for GE-EPI and SPEN at 17.2 T and 7 T, respectively). This finding was consistently observed in all animals and is summarized in Fig. 5a, which shows how increasing SPEN's repetition time from 1.5 s to 3 s decreased the number of active pixels ($p < 0.05$) from 51.5 ± 24 to 33.3 ± 22 and from 33.3 ± 20 to 17.0 ± 7.7, at 17.2 T and 7 T respectively. Such TR dependence strongly suggests that T1-related effects contribute to the fMRI SPEN signal at these high fields—particularly at 17.2 T. Also in support of a dominant T1 role for these function-related changes are the facts that both the number of activated pixels and of the activated areas signal intensity changes are lower at 7 T than at 17.2 T (Fig. 5b), as one would expect owing to the longer T1 of water at the higher field (ca. 2.5 s) than at the lower one (ca. 1.5 s on average) (de Graaf et al., 2006). It is also likely that these differences are reflecting the increased SNR achieved in the 17.2 T acquisitions. Notably, although the number of functionally active pixels changes significantly with TR, no statistically significant differences in the average signal intensity changes induced by activation were noticed for SPEN acquisitions performed at the same magnetic field but at different TRs (Fig. 5b). Also worth noting is SPEN's reduced coverage of the deeper regions of the brain; this reduction can be explained by the longer evolution times experienced by spins positioned at the edges of the brain, leading to a stronger apparent decay of their SPEN signals (see also Hyperoxia data analysis).

The influence that the SPEN fMRI activation maps show on TR (Figs. 4, 5), reflects functional-driven changes in the effective longitudinal relaxation times. These in turn could be mirroring the fact that the $SPEN_{90}$ experiment relies on a broad, full-volume excitation, coupled to flow derived effects related to an activation process that increases the volume of blood supplied to this region. Further light on the nature of potential inflow-driven contrast effects like those observed in Fig. 4, arises upon comparing the temporal responses of SPEN and EPI fMRI time courses. Preliminary data, not shown, suggest that the rising period of the $SPEN_{90}$ BOLD signal is faster than that of SE-EPI. SPEN's shorter latency period supports the idea that inflow effects have an important

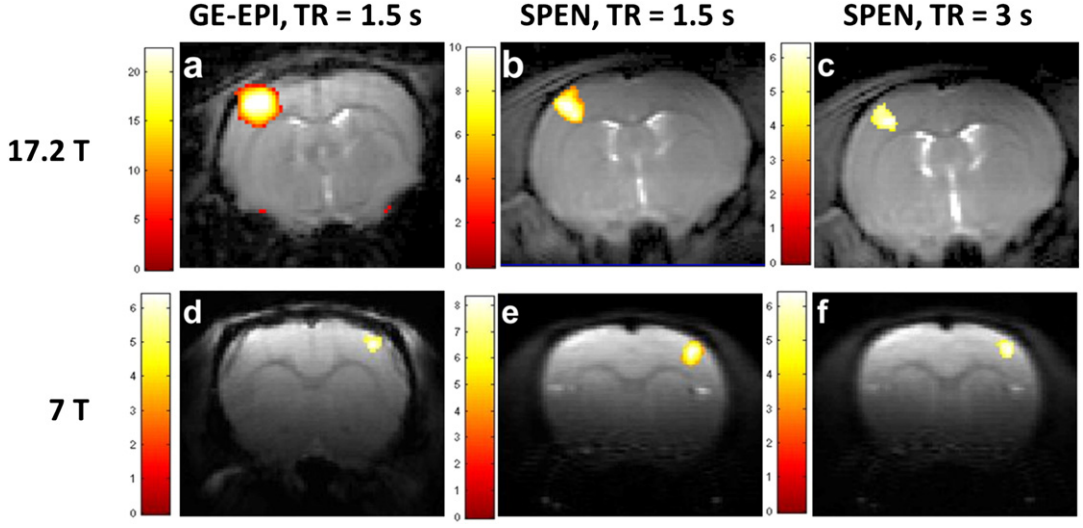

Fig. 4. fMRI statistical maps acquired at 17.2 T (a, b, c) and 7 T (d, e, f) overlaid on corresponding coronal images, collected using a GE-EPI sequence (a, d) and a 90°-based SPEN sequence with TR 1.5 s (b, e) and 3 s (c, f).

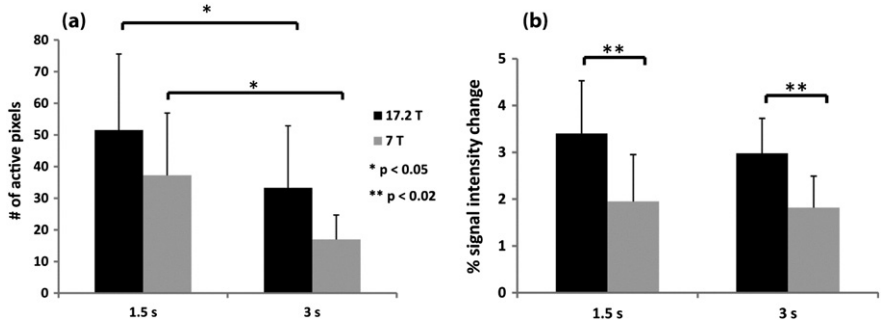

Fig. 5. Number of active pixels counted (a), and fMRI signal intensity change (b), measured at 17.2 T (black) and 7 T (gray) by SPEN fMRI for repetition times TRs of 1.5 and 3 s. The statistical comparison was done using Student paired *t* tests. Error bars represent standard deviations ($n = 8$).

influence in this method's BOLD response (Gao and Liu, 2012; Liu et al., 2008). Inflow effects could also explain why changing the TR changes the number but not the intensity of the pixels contributing to the observed activation: for voxels irrigated by larger vessels these effects would display maximum contrast even when TR = 3 s, but additionally saturated voxels would be saturated upon reducing this TR to 1.5 s.

Discussion and conclusions

Not being able to measure neural activity in certain brain regions is a restriction that has prompted substantial efforts to improve standard fMRI methods (Deichmann et al., 2003; Feinberg et al., 2010; Heidemann et al., 2012; Norris et al., 2011). This limitation becomes even more acute when the fMRI examination is performed in small animals, where the use of ultrahigh magnetic fields is more prevalent than in humans, and more essential in order to tackle the smaller dimensions that are usually dealt with. This study showed that fully-refocused SPEN-based techniques can be used as reliable methods for such high and ultra-high magnetic field fMRI, to acquire preclinical activation maps that are free from the usual effects of field imperfections and distortions. Fully refocused SPEN sequences would not be a priori evident choices for such experiments, given the built-in compensation that these sequences exhibit to B_0 inhomogeneities—and by the same token, to T2*-based BOLD effects. This T2* independence was indeed verified here with ancillary hyperoxia SPEN and SE-EPI experiments. At ultrahigh fields, however, it appears that the substantial T2 shortening that water undergoes robs T2*-based changes (and hence BOLD) from some of its lower-field contrast—and usefulness. On the other hand, the concomitant lengthening that T1 undergoes as magnetic fields increase, may provide a novel source of localized activation marking. Given the wideband chirped excitations used by such sequences, affecting not only the observed slice but also the full brain volume, $SPEN_{90}$ fMRI appeared highly sensitive to T1 effects; this was demonstrated by the dependence of the active area size on the repetition time and on the magnetic field employed. A main potential factor explaining these changes could be in-flow effects, a feature which if further substantiated could render high-field SPEN as a valuable cerebral blood volume-based fMRI technique. Compared to standard BOLD acquisitions, SPEN can therefore enable better specificity, similar to the vascular space occupancy-dependent (VASO) technique (Lu et al., 2013), overcoming in the same time the UHF challenges limiting the latter.

In summary, disentangling the different T1, T2, T2* and in-flow contributions to EPI- and SPEN-based fMRI signals, requires a careful analysis which may evidence a good complementary between many alternative imaging options at ultrahigh fields. This flexibility may prove important when seeking good image qualities, free from susceptibility or chemical shift artifacts. SPEN-based imaging sequences in particular, which have shown robustness vis-à-vis these distortions, evidenced a high functional contrast despite their T2*-free character. This makes them an attractive and interesting tool to further explore functional activation in rodents at ultrahigh magnetic fields.

Acknowledgments

LC acknowledges UNIRS Laboratory (NeuroSpin/I2BM/DSV/CEA) for partially supporting this work, and Boucif Djemai for help with animal handling. Financial support from the EU (through ERC Advanced Grant # 246754), the Kimmel Institute for Magnetic Resonance and the generosity of the Perlman Family Foundation, are gratefully acknowledged. TR acknowledged the EC Marie Curie Action ITN METAFLUX (project 264780) for a stipend. This work was also supported by grants GIS-IBISA-2010 (France) and by the Israel Science Foundation (grant 795/13).

Appendix A. Supplementary data

Supplementary data to this article can be found online at http://dx.doi.org/10.1016/j.neuroimage.2015.03.018.

References

Airaksinen, A.M., Niskanen, J.P., Chamberlain, R., Huttunen, J.K., Nissinen, J., Garwood, M., Pitkanen, A., Grohn, O., 2010. Simultaneous fMRI and local field potential measurements during epileptic seizures in medetomidine-sedated rats using raser pulse sequence. Magn. Reson. Med. 64, 1191–1199.
Bandettini, P.A., Bowtell, R., Jezzard, P., Turner, R., 2012. Ultrahigh field systems and applications at 7 T and beyond: progress, pitfalls, and potential. Magn. Reson. Med. 67, 317–321.
Ben-Eliezer, N., Frydman, L., 2011. Spatiotemporal encoding as a robust basis for fast three-dimensional in vivo MRI. NMR Biomed. 24, 1191–1201.
Ben-Eliezer, N., Shrot, Y., Frydman, L., 2010. High-definition, single-scan 2D MRI in inhomogeneous fields using spatial encoding methods. Magn. Reson. Imaging 28, 77–86.
Ben-Eliezer, N., Goerke, U., Ugurbil, K., Frydman, L., 2012. Functional MRI using super-resolved spatiotemporal encoding. Magn. Reson. Imaging 30, 1401–1408.
Ben-Eliezer, N., Shrot, Y., Frydman, L., Sodickson, D.K., 2014. Parametric analysis of the spatial resolution and signal-to-noise ratio in super-resolved spatiotemporally encoded (SPEN) MRI. Magn. Reson. Med. 72, 418–429.
Chamberlain, R., Park, J.Y., Corum, C., Yacoub, E., Ugurbil, K., Jack, C.R., Garwood, M., 2007. RASER: a new ultrafast magnetic resonance Imaging method. Magn. Reson. Med. 58, 794–799.
Chavhan, G.B., Babyn, P.S., Thomas, B., Shroff, M.M., Haacke, E.M., 2009. Principles, techniques, and applications of T2*-based MR imaging and its special applications. Radiographics 29, 1433-U1272.
Chen, Y., Li, J., Qu, X., Chen, L., Cai, C., Cai, S., Zhong, J., Chen, Z., 2013. Partial Fourier transform reconstruction for single-shot MRI with linear frequency-swept excitation. Magn. Reson. Med. 69, 1326–1336.
de Graaf, R.A., Brown, P.B., McIntyre, S., Nixon, T.W., Behar, K.L., Rothman, D.L., 2006. High magnetic field water and metabolite proton T1 and T2 relaxation in rat brain in vivo. Magn. Reson. Med. 56, 386–394.
Deichmann, R., Gottfried, J.A., Hutton, C., Turner, R., 2003. Optimized EPI for fMRI studies of the orbitofrontal cortex. Neuroimage 19, 430–441.
Feinberg, D.A., Moeller, S., Smith, S.M., Auerbach, E., Ramanna, S., Gunther, M., Glasser, M.F., Miller, K.L., Ugurbil, K., Yacoub, E., 2010. Multiplexed echo planar imaging for sub-second whole brain FMRI and fast diffusion imaging. PLoS ONE 5, e15710.
Frahm, J., Merboldt, K.-D., Hanicke, W., Kleinschmidth, A., Boecker, H., 1994. Brain or vein—oxygenation or flow? On signal physiology in functional MRI on human brain activation. NMR Biomed. 7, 45–53.

Gao, J.H., Liu, H.L., 2012. Inflow effects on functional MRI. Neuroimage 62, 1035–1039.
Goerke, U., Garwood, M., Ugurbil, K., 2011. Functional magnetic resonance imaging using RASER. Neuroimage 54, 350–360.
Gruetter, R., 1993. Automatic, localized in vivo adjustment of all first- and second-order shim coils. Magn. Reson. Med. 29, 804–811.
Heeger, D.J., Ress, D., 2002. What does fMRI tell us about neuronal activity? Nat. Rev. Neurosci. 3, 142–151.
Heidemann, R.M., Ivanov, D., Trampel, R., Fasano, F., Meyer, H., Pfeuffer, J., Turner, R., 2012. Isotropic submillimeter fMRI in the human brain at 7 T: combining reduced field-of-view imaging and partially parallel acquisitions. Magn. Reson. Med. 68, 1506–1516.
Li, Jing, Chen, Lin, Cai, Shuhui, Cai, Congbo, Zhong, Jianhui, Chen, Zhong, 2014. Imaging with referenceless distortion correction and flexible regions of interest using single-shot biaxial spatiotemporally encoded MRI. Neuroimage 105, 93–111.
Kanayama, S., Kuhara, S., Satoh, K., 1996. In vivo rapid magnetic field measurement and shimming using single scan differential phase mapping. Magn. Reson. Med. 36, 637–642.
Kim, S.-G., Hendrich, K., Hu, X., Merkle, H., Ugurbil, K., 1994. Potential pitfalls of functional MRI using conventional gradient-recalled echo techniques. NMR Biomed. 7, 69–74.
Kunz, D., 1986. Use of frequency-modulated radiofrequency pulses in MR imaging experiments. Magn. Reson. Med. 3, 377–384.
Liu, H.L., Wei, P.S., Wai, Y.Y., Kuan, W.C., Huang, C.M., Wu, C.W.W., Buckle, C., Wan, Y.L., Gao, J.H., 2008. Inflow effects on hemodynamic responses characterized by event-related fMRI using gradient-echo EPI sequences. Med. Phys. 35, 4300–4307.
Logothetis, N.K., 2008. What we can do and what we cannot do with fMRI. Nature 453, 869–878.
Logothetis, N.K., Wandell, B.A., 2004. Interpreting the BOLD signal. Annu. Rev. Physiol. 66, 735–769.
Lu, H.Z., Hua, J., van Zijl, P.C.M., 2013. Noninvasive functional imaging of cerebral blood volume with vascular-space-occupancy (VASO) MRI. NMR Biomed. 26, 932–948.
Norris, D.G., 2006. Principles of magnetic resonance assessment of brain function. J. Magn. Reson. Imaging 23, 794–807.
Norris, D.G., 2012. Spin-echo fMRI: the poor relation? Neuroimage 62, 1109–1115.
Norris, D.G., Zysset, S., Mildner, T., Wiggins, C.J., 2002. An investigation of the value of spin-echo-based fMRI using a Stroop color-word matching task and EPI at 3 T. Neuroimage 15, 719–726.
Norris, D.G., Koopmans, P.J., Boyacioglu, R., Barth, M., 2011. Power Independent of Number of Slices (PINS) radiofrequency pulses for low-power simultaneous multi-slice excitation. Magn. Reson. Med. 66, 1234–1240.
Ogawa, S., Lee, T.M., 1990. Magnetic-resonance-imaging of blood-vessels at high fields—in vivo and in vitro measurements and image simulation. Magn. Reson. Med. 16, 9–18.
Ogawa, S., Menon, R.S., Tank, D.W., Kim, S.G., Merkle, H., Ellermann, J.M., Ugurbil, K., 1993. Functional brain mapping by blood oxygenation level-dependent contrast magnetic-resonance-imaging—a comparison of signal characteristics with a biophysical model. Biophys. J. 64, 803–812.
Pipe, J.G., 1995. Spatial encoding and reconstruction in MRI with quadratic phase profiles. Magn. Reson. Med. 33, 24–33.
Schmidt, R., Frydman, L., 2014. New spatiotemporal approaches for fully refocused, multislice ultrafast 2D MRI. Magn. Reson. Med. 71, 711–722.
Schwarzbauer, C., Mildner, T., Heinke, W., Brett, M., Deichmann, R., 2010. Dual echo EPI—the method of choice for fMRI in the presence of magnetic field inhomogeneities? Neuroimage 49, 316–326.
Tal, A., Frydman, L., 2010. Single-scan multidimensional magnetic resonance. Prog. Nucl. Magn. Reson. Spectrosc. 57, 241–292.
Ugurbil, K., 2012. The road to functional imaging and ultrahigh fields. Neuroimage 62, 726–735.
Ugurbil, K., Hu, X.P., Chen, W., Zhu, X.H., Kim, S.G., Georgopoulos, A., 1999. Functional mapping in the human brain using high magnetic fields. Philos. Trans. R. Soc. Lond. Ser. B Biol. Sci. 354, 1195–1213.
Weiskopf, N., Hutton, C., Josephs, O., Deichmann, R., 2006. Optimal EPI parameters for reduction of susceptibility-induced BOLD sensitivity losses: a whole-brain analysis at 3 T and 1.5 T. Neuroimage 33, 493–504.